Check for updates

iMRI

Investigative Magnetic Resonance Imaging

Diagnostic Value of Susceptibility-Weighted MRI in Differentiating Cerebellopontine Angle Schwannoma from Meningioma

Minkook Seo, Yangsean Choi, Song Lee, Bum-soo Kim, Jinhee Jang, Na-Young Shin, So-Lyung Jung, Kook-Jin Ahn

Department of Radiology, Seoul St. Mary's Hospital, College of Medicine, The Catholic University of Korea, Seoul, Korea

Original Article

Background: Differentiation of cerebellopontine angle (CPA) schwannoma from meningioma is often a difficult process to identify.
Purpose: To identify imaging features for distinguishing CPA schwannoma from meningioma and to investigate the usefulness of susceptibility-weighted imaging (SWI) in differentiating them.
Materials and Methods: Between March 2010 and January 2015, this study pathologically confirmed 11 meningiomas and 20 schwannomas involving CPA with preoperative SWI were retrospectively reviewed. Generally, the following MRI features were evaluated: 1) maximal diameter on axial image, 2) angle between tumor border and adjacent petrous bone, 3) presence of intratumoral dark signal intensity on SWI, 4) tumor consistency, 5) blood-fluid level, 6) involvement of internal auditory canal (IAC), 7) dural tail, and 8) involvement of adjacent intracranial space. On CT, 1) presence of dilatation of IAC, 2) intratumoral calcification, and 3) adjacent hyperostosis were evaluated. All features were compared using Chi-squared tests and Fisher's exact tests. The univariate and multivariate logistic regression analysis were performed to identify imaging features that differentiate both tumors.
Results: The results noted that schwannomas more frequently demonstrated dark spots on SWI (P = 0.025), cystic consistency (P = 0.034), and globular angle (P = 0.008); schwannomas showed more dilatation of internal auditory meatus and lack of calcification (P = 0.008 and P = 0.02, respectively). However, it was shown that dural tail was more common in meningiomas (P < 0.007). In general, dark spots on SWI and dural tail remained significant in multivariate analysis (P = 0.037 and P = 0.012, respectively). In this case, the combination of two features showed a sensitivity and specificity of 80% and 100% respectively, with an area under the receiver operating characteristic curve of 0.9.
Conclusion: In conclusion, dark spots on SWI were found to be helpful in differentiating CPA schwannoma from meningioma. It is noted that combining dural tail with dark spots on SWI yielded strong diagnostic value in differentiating both tumors.

Keywords: Meningioma; Vestibular schwannoma; Susceptibility-weighted imaging; Magnetic resonance imaging; Cerebellopontine angle tumors

iMRI

INTRODUCTION

Broadly speaking, meningioma and schwannoma are the most common and 2nd most common extra axial tumors in adults, respectively. Considering MRI is the modality of choice for presurgical imaging with excellent tissue characterization, multiplanar capability without the risk of radiation, preoperative differentiation of both tumors on MRI would be clinically beneficial.

In general, microhemorrhage occurs more often in schwannomas, while it is noted that the incidence of calcification is more common in meningioma (1). On MRI, meningiomas frequently have dural tail sign, calcification, and broad base on the petrous bone; meningiomas abutting the internal auditory canal (IAC) cause hyperostosis of adjacent bone. On the contrary, schwannomas have close contact with cranial nerves, typically involve IAC with widening of the canal, and display cystic changes and globular angle with petrous bone.

However, in some cases they share similar imaging features, posing challenges to radiologists; approximately 25% of cerebellopontine angle (CPA) meningiomas are reportedly misdiagnosed for schwannoma (2). A specific imaging feature such as blood-fluid levels in schwannomas was reportedly associated with a less favorable surgical outcome (3), adding complexities to treatment planning for the patients. There has been a report that intratumoral microhemorrhages on T2* weighted gradient-echo (GRE) imaging had diagnostic potential of differentiating them (4). Similar to T2* weighted GRE imaging, susceptibility-weighted image (SWI) is capable of detecting microhemorrhages, which are seen as blooming of dark signal intensities on SWI (5). To date, there is a paucity of literature that have applied SWI in differentiating CPA schwannomas from meningiomas (6). In this relation, we hypothesized that SWI would yield meaningful diagnostic value to the conventional imaging findings, that could be useful in distinguishing CPA schwannoma from meningioma.

The purpose of this study was to evaluate the potential diagnostic value of SWI combined with conventional imaging findings on MRI and CT, as used in differentiating CPA schwannoma from meningioma for the purposes of diagnosis of patients exhibiting these conditions.

MATERIALS AND METHODS

Study Population

This retrospective study was approved by the Institutional Review Boards of our institution and informed consent was waived. Between March 2010 and January 2015, 44 patients who underwent surgery for CPA tumors were retrospectively reviewed for this study (17 meningiomas and 27 schwannomas). It is noted that the inclusion criteria for eligible patients were: 1) available pre-operative MRI with SWI sequence and CT; and 2) tumor size of at least 2.0 cm in maximal diameter for appropriate analysis. In this case, thirteen patients were excluded for the following reasons: 1) lack of pre-operative CT images (n = 5); 2) lack of pre-operative SWI sequence (n = 6); 3) tumors less than 2.0 cm in largest diameter (n = 2). Additionally, we included 11 patients with meningiomas and 20 patients with schwannomas, all with preoperative SWI and CT images.

MRI Acquisition

This brings us to understand that all images were acquired using a 3.0 Tesla MR scanner (Verio; Siemens, Erlangen, Germany). In these terms, the sequences were obtained in the following order: T1- and T2-weighted, fluid-attenuated inversion recovery (FLAIR) imaging, SWI and finally contrast-enhanced T1-weighted imaging with intravenous injection of Gadobutrol (Gadovist; Bayer, Leverkusen, Germany) at 0.1 mg/kg. SWI was acquired with 3-dimensional gradient echo sequence with flow compensation. The parameters for SWI were: field of view, 230 × 173; matrix, 256 × 192; voxel size, 0.9 × 0.9 × 2.0 mm; flip angle, 15 degree; and time repetition/echo time, 28/20 msec. In the meantime, the magnitude and phase images were simultaneously obtained from which SWI was constructed in operation of magnitude and phase images (7). The parameters for other sequences were: 1) T2-weighted imaging (repetition time [TR], 3300 msec; echo time [TE], 93 msec; flip angle [FA], 150; field of view [FOV], 210 × 210 mm; acquired matrix, 448 × 358; number of excitations [NEX], 1; echo train length [ETL], 17; section thickness, 5 mm), 2) FLAIR (TR, 9000 msec; TE, 95 msec; FA, 90; FOV, 210 × 210 mm; acquired matrix, 384 × 307; NEX, 1; ETL, 17; section thickness, 5 mm) and 3) T1-weighted and gadolinium-enhanced T1-weighted imaging (TR, 250 msec; TE, 3.0 msec; FA, 70; FOV, 210 × 210 mm; acquired matrix, 448 × 358; NEX, 2; ETL, 1; section thickness, 5 mm). Likewise, the acquired CT images were non-contrast enhanced temporal bone CT scans with slice thickness of 1.0 mm and peak kilovoltage of 120.0

(SOMATOM Definition, Siemens Healthineers, Erlangen, Germany).

Image Analysis

For all patients, MRI features were analyzed as following: 1) maximal diameter on axial image, 2) angle between tumor border and adjacent petrous bone, 3) presence of intratumoral dark signal intensity on SWI, 4) tumor consistency, 5) blood-fluid level, 6) involvement of IAC, 7) dural tail, and 8) involvement of adjacent intracranial space. It is noted that the grade of intratumoral dark spots was defined as none, < 50% (less than 50% of tumor area), and ≥ 50% (greater than or equal to 50% of tumor area). Next, the following CT features were also analyzed: 1) presence of dilatation of internal auditory meatus, 2) intratumoral calcification, and 3) adjacent hyperostosis. Then, by comparing SWI and CT images, among intratumoral dark spots on SWI, those not corresponding to calcification on CT were recorded. Additionally, all images were analyzed by two board-certified radiologists (blinded and blinded, with 6 and 25 years of experience in neuroradiology) who were noted to be in consensus regarding the results. Additionally, histologic consistencies of all tumors were reviewed from electronic medical records of our institution.

Statistical Analysis

A Pearson's Chi-squared test or Fisher's exact was performed, where appropriate, for categorized variables of imaging features and independent t-test was used for comparing continuous variables. Additionally, a univariate and multivariate logistic regression analyses were performed using imaging features. It was shown that there were noted significant variables in multivariate analysis were used to plot a receiver operating characteristics (ROC) curve. Additionally, the area under the ROC curve (AUC) was calculated from a training set consisting of 20 patients. To minimize overfitting, the multivariate logistic regression was applied to a test set consisting of 11 patients after 10-fold cross-validation, of which the best-performing model was chosen. Next, both train and test sets were randomly chosen from the entire cohort with maintaining equal proportion of both tumors. It is emphasized that all statistical analyses were performed using R statistical software (version 3.4.4, Vienna, Austria). A P-value of less than 0.05 was considered to indicate statistical significance in this case as reviewed.

RESULTS

Baseline Characteristics of Patients

In this context, the baseline clinical and tumor characteristics of all patients are summarized in Table 1. There were no significant differences as noted in characteristics, or were seen between both tumors (all Ps > 0.05). Of the 20 patients with schwannoma, 10 were women (50%) while among the 11 patients with meningioma, 7 were women (63.6%) (P = 0.724). It was shown that the mean age was 61.5 ± 12.3 years for meningioma and 51.7 ± 18.5 years for schwannoma (P = 0.125).

Comparison of Imaging Characteristics

In this respect, the detailed imaging features of both tumors are summarized in Table 2. The mean maximal diameter of schwannomas was 3.8 ± 1.3 cm while that of meningiomas was 4.2 ± 1.4 cm (P = 0.125). Here the intratumoral dark spots on SWI-not corresponding to calcific densities on CT-were more frequently observed in schwannomas (18 of 20, 90%) than in meningiomas (5 of 11, 45.5%, P = 0.025). In terms of 20 schwannomas, 13 patients (65%) had both solid and cystic components while only 2 patients (2 of 11, 18%) with meningiomas had both solid and cystic components (P = 0.034). It was noted that only schwannomas showed blood-fluid levels on MRI (P = 0.474). The IAC involvement tended to be more common in schwannomas (14 of 20, 70%) than in meningiomas (3 of 11, 27.3%) (P = 0.056). Next, the dural tail signs were more frequently seen in meningiomas (6 of 11, 54.5%) than in schwannomas (1 of 20, 5%; P = 0.007). Additionally, the schwannomas showed more globular angles between tumor with adjacent petrous bone (15 of 20, 75%) than in meningiomas (2 of 11, 18.2%; P = 0.008). On a review

Table 1. Baseline Characteristics of Patients and Tumors (n = 31)

Characteristics	Meningioma (n = 11)	Schwannoma (n = 20)	P-value
Sex, n (%)			0.724
Female	7 (63.6%)	10 (50.0%)	
Male	4 (36.4%)	10 (50.0%)	
Age, mean ± SD	61.5 ± 12.3	51.7 ± 18.5	0.125
Tumor location, n (%)			0.248
Left	4 (36.4%)	13 (65.0%)	
Right	7 (63.6%)	7 (35.0%)	

SD = standard deviation

of the preoperative CT images, intratumoral calcifications were seen in meningiomas (4 of 11, 36.4%) and none in schwannomas (0%, P = 0.02). Next, the dilatation of internal auditory meatus was only seen in schwannomas (11 of 20, 55%; P = 0.002) as well as hyperostosis of peritumoral bone (2 of 20, 10%; P = 0.749). The representative MRI of both tumors are depicted in Figure 1.

Univariate and Multivariate Logistic Regression Analysis

There are significant variables from univariate and multivariate analysis that are summarized in Table 3. In univariate analysis, dark spots on SWI, tumor consistency, IAC component, dural tail sign, and angle between tumor and adjacent petrous bone were found to be significant (P = 0.005-0.029). Among these, three variables (dark spots on SWI, IAC component, and dural tail sign) were selected for multivariate analysis, in which dark spots on SWI and dural tail sign remained significant (P = 0.037 and P = 0.012, respectively). Additionally, these two variables showed a sensitivity of 80% and a specificity of 100% with an AUC of 0.9 (Fig. 2) in differentiating schwannomas from meningiomas.

DISCUSSION

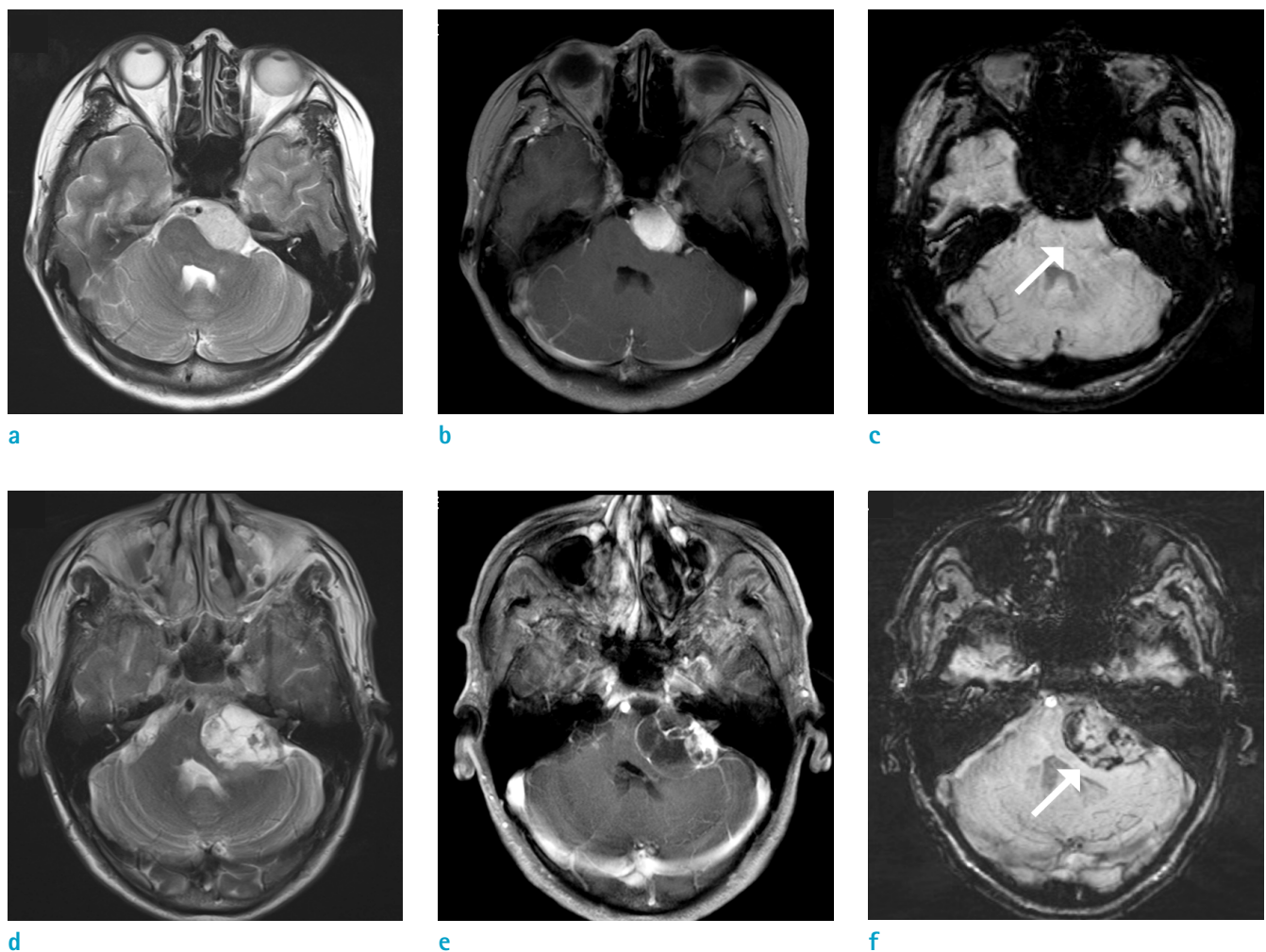In the CPA, it is known that schwannomas and

Fig. 1. Representative images of meningioma (upper row) in a 35-year-old woman and schwannoma (bottom row) in a 66-year-old male. From left to right, each column represents T2-weighted (a, d), contrast-enhanced T1-weighted (b, e) and SWI (c, f) of tumor located in left cerebellopontine angle. Schwannoma shows punctate dark signal intensities on SWI (f) while meningioma shows none (c) (arrows). SWI = susceptibility-weighted image.

meningiomas are the most common tumors that are often difficult to distinguish (8, 9). That being said, the preoperative differentiation of both tumors on imaging is important, because the operative approach and post-

Table 2. Comparison of Imaging Features of Tumors

MRI features, n (%)	Meningioma (n = 11)	Schwannoma (n = 20)	P-value
Maximal tumor diameter (cm), mean ± SD	4.2 ± 1.4	3.8 ± 1.3	0.373
Dark spot on SWI[b]			0.025
none	6 (54.5%)	2 (10.0%)	
< 50%	4 (36.4%)	14 (70.0%)	
≥ 50%	1 (9.1%)	4 (20.0%)	
Tumor consistency			0.034
Solid	9 (81.8%)	7 (35.0%)	
Solid and cystic	2 (18.2%)	13 (65.0%)	
Blood–fluid level			0.474[a]
Absent	11 (100.0%)	17 (85.0%)	
Present	0 (0.0%)	3 (15.0%)	
IAC component			0.056
Absent	8 (72.7%)	6 (30.0%)	
Present	3 (27.3%)	14 (70.0%)	
Dural tail sign			0.007
Absent	5 (45.5%)	19 (95.0%)	
Present	6 (54.5%)	1 (5.0%)	
Angle[c]			0.008
Broad	9 (81.8%)	5 (25.0%)	
Globular	2 (18.2%)	15 (75.0%)	
CT imaging features, n (%)			
Meatus dilatation			0.008[a]
Absent	11 (100.0%)	9 (45.0%)	
Present	0 (0.0%)	11 (55.0%)	
Calcification			0.02[a]
Absent	7 (63.6%)	20 (100.0%)	
Present	4 (36.4%)	0 (0.0%)	
Hyperostosis			0.749[a]
Absent	11 (100.0%)	18 (90.0%)	
Present	0 (0.0%)	2 (10.0%)	

[a]Fisher's exact test; other categorical comparisons by Pearson's Chi-squared tests
[b]Proportion of dark spot on susceptibility-weighted imaging out of total tumor area
[c]Angle between tumor and adjacent petrous bone
IAC = internal auditory canal; SWI = susceptibility-weighted imaging

treatment management differ for both tumors (10). In this context, in patients with meningiomas, postoperative hearing preservation tends to be better than schwannomas; however, recurrence incidence is higher in patients with meningiomas (9, 10). For this reason, the current study demonstrated the diagnostic value of SWI in differentiating CPA schwannoma from meningioma. Our results showed that combining dark spots on SWI with dural tail were found to be helpful in differentiating of CPA schwannoma from meningioma.

In previous studies, several CT and MRI findings for differentiating both tumors have been investigated with some success. Through this lens, imaging features favoring the diagnosis of schwannoma include globular shape of a tumor, IAC component, and an acute angle between tumor with the adjacent petrous bone (11, 12). On the other hand, imaging features favoring the diagnosis of meningiomas include sessile shape with a broad base against petrous bone, an obtuse angle with the petrous temporal bone, dural tail sign, intratumoral calcification and hyperostotic changes (8, 11-14). Furthermore, in line with previous findings, the univariate logistic analysis of this study showed that dural tail sign, the angle between tumor with adjacent bone, and IAC dilatation were found to be significant features in distinguishing both tumors.

In this relation, the results of this study showed that 65% of schwannomas showed mixed solid and cystic appearances, which is higher than the previously reported incidences of cystic schwannomas (5.7% to 48%) (15-17). Unlike a previous study that reported 53% of blood-fluid levels on preoperative MRI in schwannomas (3), this study showed only 15% schwannomas with internal blood-fluid levels. Upon review, this difference may be attributable to the larger sample size of their study (131 schwannomas vs. 20 schwannomas). In both univariate and multivariate analysis, intratumoral dark spots on SWI and dural tail sign were significant imaging features for differentiating schwannoma from meningioma in CPA. Considering dural tail sign can be assessed on conventional imaging (i.e. contrast-enhanced CT or MRI), the use of SWI for detecting intratumoral dark spots-or microhemorrhages-was found to have a diagnostic value.

It is emphasized that advances in MRI technology have led to improved sensitivity for detecting a byproduct of microbleeding, called hemosiderin. In these cases, microhemorrhage appears as round hypointense foci on both conventional GRE images and SWI (18). Recently, SWI is increasingly used routinely in clinical practice as

Table 3. Univariate and Multivariate Logistic Regression Analysis Using Clinical and Imaging Characteristics

Variables	Univariate analysis		Multivariate analysis[a]	
	OR (95% CI)	P-value	OR (95% CI)	P-value
Age	0.96 [0.91, 1.0]	0.13		
Sex, male	1.75 [0.4, 8.52]	0.467		
Maximal tumor diameter	0.76 [0.42, 1.36]	0.362		
Dark spot on SWI (none vs. present)	2.73 [1.27, 6.98]	0.017	3.25 [1.19, 12]	0.037
Tumor consistency	8.36 [1.61, 65.9]	0.02		
Blood-fluid level		0.994		
IAC component	6.22 [1.31, 37.0]	0.029	2.94 [0.32, 30.5]	0.331
Dural tail sign	0.04 [0, 0.33]	0.009	0.03 [0, 0.33]	0.012
Angle[b]	13.5 [2.5, 111.6]	0.005		
Meatus dilatation		0.995		
Calcification		0.995		
Hyperostosis		0.995		

[a]Variables with $P < 0.02$ were further analyzed in multivariate analysis
[b]Angle formed between tumor margin and adjacent petrous bone
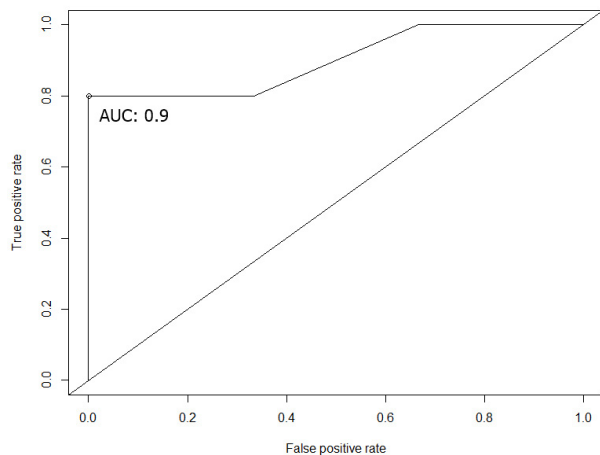CI = confidence interval; OR = odds ratio

Fig. 2. A receiver operator characteristic curve based on two significant imaging features from multivariate logistic regression-dark spots on SWI and dural tail sign. At the optimal threshold point (open circle), the AUC was 0.9 with a sensitivity and a specificity of 80% and 100%, respectively. AUC = area under the receiver operator characteristic curve.

it maximizes the sensitivity to susceptibility effects by combining long echo time and a fully flow-compensated 3D GRE sequence, making it superior to the conventional T2* GRE. In addition, because of its high resolution and phase information, it is noted that SWI is more sensitive in detecting microhemorrhages compared to the conventional GRE (19). Additionally, one study reported that SWI detected 67% more cerebral microbleeds than the conventional GRE sequence (20). Capability of microhemorrhage detection on imaging is important, since intratumoral microhemorrhage is a well-known pathologic characteristic of schwannomas (21, 22).

In this respect, only a few studies have reported the diagnostic value of microhemorrhages in CPA schwannomas on MRI (4, 6, 22, 23). The Park et al. (23) study reported that they detected microhemorrhage in 35% of CPA schwannomas by using T2-weighted sequence; however, all cases were confirmed to have hemosiderin by histopathologic examination. In our study, among the 18 schwannomas with dark spots on SWI, only three showed spots of signal voids on T2-weighted image, suggesting superior sensitivity of SWI in detecting microhemorrhages than T2-weighted sequence. Similar to our study, it is important to reiterate that Mishra et al. (24) applied SWI for differentiating CPA schwannomas from meningiomas, and found that SWI showed a sensitivity and specificity of 100% and 92%, respectively in differentiating the two.

Generally speaking, the diagnostic value of intratumoral microhemorrhage on MRI for distinguishing CPA schwannoma from meningiomas have been previously investigated using conventional GRE (4) and PRESTO

(principles of echo shifting with a train of observation) sequence (6) with histopathologic correlation. In other words, the PRESTO sequence was developed to make rapid T2*-weighted scanning (25), which is used for perfusion and functional MRI (26). However, more susceptibility artifacts in the lower parts of the brain were seen for PRESTO sequence due to longer echo time compared to SWI (27), suggesting SWI may be more applicable for assessing microhemorrhages in the CPA.

Upon review, our study has a few limitations in addition to the inherent bias associated with retrospective design. First, the results from a small sample size of 31 patients might not be generalizable to other cohorts, and may need a larger participation group. Additionally, dark spots on SWI were considered as microhemorrhages after correlating with CT images; pathologic confirmation from surgical specimen could have added definitive meaning to the dark spots on SWI. Furthermore, it is noted that microhemorrhages could have been differentiated from calcifications via phase images acquired for processing SWI; in doing so, SWI could have distinguished calcifications (i.e. diamagnetic) from microhemorrhages (i.e. paramagnetic). However, in reviewing the collected data, the raw phase images were not readily available. For this reason, future studies would need to investigate the value of phase images of SWI for this purpose.

In conclusion, on top of the conventional imaging findings of CPA meningiomas and schwannomas, the intratumoral dark spots on SWI were found to be a useful feature for differentiating both tumors, suggesting its potential diagnostic value for the future. Furthermore, combining dural tail sign with dark spots on SWI resulted in improved differentiation in both types of tumors.

Acknowledgments

Declaration of Conflicting Interests

None declared.

Funding

REFERENCES

1. Schlieter M, Zoubaa S, Kress B, Unterberg A, Jacobi C, Hahnel S. Hemorrhagic acoustic schwannoma: radiological and histopathological findings. J Neuroradiol 2005;32:210-212

2. Grey PL, Moffat DA, Hardy DG. Surgical results in unusual cerebellopontine angle tumours. Clin Otolaryngol Allied Sci 1996;21:237-243

3. Xia L, Zhang H, Yu C, et al. Fluid-fluid level in cystic vestibular schwannoma: a predictor of peritumoral adhesion. J Neurosurg 2014;120:197-206

4. Thamburaj K, Radhakrishnan VV, Thomas B, Nair S, Menon G. Intratumoral microhemorrhages on T2*-weighted gradient-echo imaging helps differentiate vestibular schwannoma from meningioma. AJNR Am J Neuroradiol 2008;29:552-557

5. Liang L, Korogi Y, Sugahara T, et al. Detection of intracranial hemorrhage with susceptibility-weighted MR sequences. AJNR Am J Neuroradiol 1999;20:1527-1534

6. Tomogane Y, Mori K, Izumoto S, et al. Usefulness of PRESTO magnetic resonance imaging for the differentiation of schwannoma and meningioma in the cerebellopontine angle. Neurol Med Chir (Tokyo) 2013;53:482-489

7. Haacke EM, Xu Y, Cheng YC, Reichenbach JR. Susceptibility weighted imaging (SWI). Magn Reson Med 2004;52:612-618

8. Zamani AA. Cerebellopontine angle tumors: role of magnetic resonance imaging. Top Magn Reson Imaging 2000;11:98-107

9. Nakamura M, Roser F, Dormiani M, Matthies C, Vorkapic P, Samii M. Facial and cochlear nerve function after surgery of cerebellopontine angle meningiomas. Neurosurgery 2005;57:77-90; discussion 77-90

10. Voss NF, Vrionis FD, Heilman CB, Robertson JH. Meningiomas of the cerebellopontine angle. Surg Neurol 2000;53:439-446; discussion 446-437

11. Tong KA, Harnsberger HR, Swartz JD. The vestibulocochlear nerve, emphasizing the normal and diseased internal auditory canal and cerebellopontine angle. In Swartz JD, Harnsberger HR, eds. Imaging of the temporal bone. 3rd ed. New York: Thieme, 1998:394-472

12. Lalwani AK, Jackler RK. Preoperative differentiation between meningioma of the cerebellopontine angle and acoustic neuroma using MRI. Otolaryngol Head Neck Surg 1993;109:88-95

13. Ryoo JW, Na DG, Woo JY, et al. Investigation of juxtasellar and cerebellopontine angle meningiomas and neurogenic tumours: two-phase helical CT. Neuroradiology 2001;43:637-643

14. Mikhael MA, Ciric IS, Wolff AP. Differentiation of cerebellopontine angle neuromas and meningiomas with MR imaging. J Comput Assist Tomogr 1985;9:852-856

15. Piccirillo E, Wiet MR, Flanagan S, et al. Cystic vestibular schwannoma: classification, management, and facial nerve outcomes. Otol Neurotol 2009;30:826-834

16. Schober R, Vogeley KT, Urich H, Holzle E, Wechsler W. Vascular permeability changes in tumours of the peripheral nervous system. Virchows Arch A Pathol Anat Histopathol 1992;420:59-64

17. Jeng CM, Huang JS, Lee WY, Wang YC, Kung CH, Lau MK. Magnetic resonance imaging of acoustic schwannomas. J Formos Med Assoc 1995;94:487-493

18. Werring DJ. Cerebral microbleeds: clinical and pathophysiological significance. J Neuroimaging 2007;17:193-203

19. Akter M, Hirai T, Hiai Y, et al. Detection of hemorrhagic hypointense foci in the brain on susceptibility-weighted imaging clinical and phantom studies. Acad Radiol 2007;14:1011-1019

20. Nandigam RN, Viswanathan A, Delgado P, et al. MR imaging detection of cerebral microbleeds: effect of susceptibility-weighted imaging, section thickness, and field strength. AJNR Am J Neuroradiol 2009;30:338-343

21. Russell DS, Rubinstein LJ. Tumors of meninges and related tissues, tumors of cranial, spinal and peripheral nerve sheaths. In Bigner DD, McLendon RE, Bruner JM, eds. Russell and Rubinstein's pathology of tumors of the nervous system. 6th ed. London: Arnold, 1998:67-194

22. Ishii K, Takahashi S, Matsumoto K, et al. Hemorrhage and abnormal veins in acoustic neurinoma: MR findings. Radiat Med 1996;14:65-69

23. Park CK, Kim DC, Park SH, et al. Microhemorrhage, a possible mechanism for cyst formation in vestibular schwannomas. J Neurosurg 2006;105:576-580

24. Mishra A, Thomas B, Kapilamoorthy TR. Susceptibility weighted imaging – a problem-solving tool in differentiation of cerebellopontine angle schwannomas and meningiomas. Neuroradiol J 2017;30:253-258

25. Liu G, Sobering G, Duyn J, Moonen CT. A functional MRI technique combining principles of echo-shifting with a train of observations (PRESTO). Magn Reson Med 1993;30:764-768

26. Chavhan GB, Babyn PS, Thomas B, Shroff MM, Haacke EM. Principles, techniques, and applications of T2*-based MR imaging and its special applications. Radiographics 2009;29:1433-1449

27. Eriksson S. A study of susceptibility-weighted MRI including a comparison of two different implementations. Sweden: Lund University, 2011